

A Digital Switch and Femto-Tesla Magnetic Field Sensor Based on Fano Resonance in a Spin Field Effect Transistor

J. Wan, M. Cahay*

Department of Electrical and Computer Engineering
University of Cincinnati, Cincinnati, Ohio 45221, USA

S. Bandyopadhyay

Department of Electrical and Computer Engineering
Virginia Commonwealth University, Richmond, Virginia 23284, USA

Abstract

We show that a Spin Field Effect Transistor, realized with a semiconductor quantum wire channel sandwiched between *half-metallic* ferromagnetic contacts, can have Fano resonances in the transmission spectrum. These resonances appear because the ferromagnets are half-metallic, so that the Fermi level can be placed above the majority but below the minority spin band. In that case, the majority spins will be propagating, but the minority spins will be evanescent. At low temperatures, the Fano resonances can be exploited to implement a digital binary switch that can be turned on or off with a very small gate voltage swing of few tens of μV , leading to extremely small dynamic power dissipation during switching. An array of $500,000 \times 500,000$ such transistors can detect ultrasmall changes in a magnetic field with a sensitivity of 1 femto-Tesla/ \sqrt{Hz} , if each transistor is biased near a Fano resonance.

*Corresponding author. E-mail: marc.cahay@uc.edu

1 Introduction

Despite the fact that the first Spin Field Effect Transistor (SPINFET) was proposed almost two decades ago [1], and numerous clones have appeared since then [2, 3, 4], no SPINFET has ever been experimentally demonstrated. The primary obstacle to experimental demonstration is the inability to achieve high spin injection efficiency at the interface between the source and channel, and high spin detection efficiency at the interface between the channel and drain. The spin injection efficiency is critical in determining the transistor performance. For example, it can be easily shown that the maximum ratio of the on-conductance to off-conductance of the transistor is [5]

$$\frac{G_{on}}{G_{off}} = \frac{1 + \zeta_S \zeta_D}{1 - \zeta_S \zeta_D} \quad (1)$$

where ζ_S is the spin injection efficiency at the source/channel interface and ζ_D is the spin detection efficiency at the drain/channel interface. Consequently, in order to achieve a on-off conductance ratio of 10^5 , typical of modern transistors, the spin injection and detection efficiencies have to be as large as 99.9995%, which is an extremely tall order.

The maximum spin injection efficiency demonstrated to date is 90% at low temperatures [6]. With that value, the conductance on-off ratio is a mere 9.5 - a far cry from 10^5 . In other words, the conductance modulation is critically dependent on spin injection efficiency. Therefore, well-engineered SPINFETs should have excellent spin injection and detection efficiencies.

Half metallic ferromagnets [7, 8, 9], in which carriers at the Fermi level have only one spin (majority spin), are the optimum electrical spin injectors. They are often invoked as the most promising route to achieving nearly 100% spin injection efficiency. Here, we report our investigation of Spin Field Effect Transistors with half metallic source and drain contacts. An example could be an InAs channel with Lanthanum Strontium Manganate (LSMO) contacts, which are known to have very high degree of spin polarization at low temperatures and approximate ideal half metals. We restrict ourselves to a quantum wire

channel since it is known to produce maximum conductance modulation [1].

We have studied *ballistic* spin transport through this device by solving the Pauli equation, which yields the transmission amplitudes of both majority and minority spins in the source contact. Assumption of ballistic transport is realistic since mobility in quantum wire channels can be reasonably high. We also neglect spin relaxation in the channel since the Elliott-Yafet mechanism [10] requires carrier scattering (which is assumed to be absent in ballistic models) and the D'yakonov-Perel' mechanism [11] is absent in a quantum wire channel where only one subband is occupied. Finally, we neglect any scattering at the interface between the ferromagnet and semiconductor, which can cause spin relaxation.

With the above model, we have studied spin dependent transmission spectra of electrons through the SPINFET. Our study revealed the existence of Fano resonances in the transmission spectra since the Fermi level in the device can be located above the majority spin band in the source (which contributes propagating electrons), but below the minority spin band (which is evanescent). It is well known that such a situation causes Fano resonances [12]. We found that the Fano resonances are narrow and well-resolved at sufficiently low temperatures. We can therefore bias the transistor around such a resonance (by applying an appropriate dc gate voltage), so that a small change in the gate voltage will vary the electron injection energy around the Fano resonance and switch the transmission through the device from maximum to minimum. This is the basis of a digital 'switch' which can be switched on and off with a very small gate voltage swing, resulting in extremely small dynamic power dissipation during switching.

We also considered the situation when the transistor is placed in a static magnetic field directed along the channel. As long as the transistor is biased near a Fano resonance, a small change in the magnetic field can change the transmission through the device (and therefore the channel conductance) from maximum to nearly zero. Thus, this device is capable of detecting minute changes in a magnetic field. We show that an appropriately designed system can detect magnetic field changes with a sensitivity of $\sim 1 \text{ femtoTesla}/\sqrt{Hz}$.

This paper is organized as follows. In the next Section, we present the theory. In Section 3, we present results and in Section 4, we present calculations of the sensitivity of a magnetic field sensor based on this principle. The conclusions are presented in Section 5.

2 Theory

Consider a Spin Field Effect Transistor (Spin FET) with half-metallic ferromagnetic source and drain contacts, as shown in Fig. 1(a). The channel is a quantum wire in which only the lowest subband is occupied by carriers. The conduction band discontinuity at the heterointerface between the channel and the gate insulator results in an effective electric field along the y-axis, which induces a Rashba spin orbit interaction in the channel. The ferromagnetic contacts induce a static magnetic field in the x-direction. This field can also be applied with external sources.

The equilibrium energy band diagram along the channel (x-direction) is shown in Fig. 1(b). We adopt the Stoner model and assume that the majority and minority spin bands in the ferromagnets are exchange split by an amount Δ . The Fermi level is below the bottom of the minority spin band so that the spin polarization of carriers at the Fermi energy in the ferromagnets is 100% (hence “half metallic”). The majority spins from the ferromagnet will be *propagating* and the minority spins will be *evanescent*. For the sake of simplicity, we will neglect space charge effects and assume that the conduction band edge in the channel is flat and invariant in the x-coordinate. Furthermore, the contact potentials at the contact/channel interface will be represented by two delta barriers of height Γ .

If we assume that the confinement potential in the z-direction is parabolic and given by $V(z) = (1/2)m^*\omega_0^2z^2$, then the approximate energy dispersion relations of the lowest spin split subbands in the channel (derived using perturbation theory) are given by [13, 14, 15]

$$E_1(k_x) = \frac{1}{2}\hbar\omega + \Delta E_c + \frac{\hbar^2 k_x^2}{2m^*} - \sqrt{(\eta k_x)^2 + \left(\frac{g^* \mu_B B}{2}\right)^2}, \quad (2)$$

$$E_2(k_x) = \frac{1}{2}\hbar\omega + \Delta E_c + \frac{\hbar^2 k_x^2}{2m^*} + \sqrt{(\eta k_x)^2 + \left(\frac{g^* \mu_B B}{2}\right)^2}, \quad (3)$$

where the subscripts ‘1’ and ‘2’ refer to the lower and upper subbands, $\omega = \sqrt{\omega_0^2 + \omega_c^2}$, $\omega_c = eB/m^*$, g^* is the effective Landé g-factor in the channel, k_x is the wavevector component in the x-direction, m^* is the effective mass of carriers, and η is the strength of the Rashba interaction. The quantity ΔE_c is the potential barrier between the ferromagnets and the channel, and includes the confinement energy due to confinement in the y-direction (see Fig. 1(b)).

If the axial magnetic field B is below a critical field $B_c (= 4 \eta m^* / (\hbar^2 g \mu_B))$, then the dispersion relation $E_1(k_x)$ will have a camel-back shape with a local maximum at $k_x = 0$ and two local minima at $k_x = \pm(\sqrt{4\eta^2(m^*)^2/\hbar^4 - (g^*\mu_B B)^2/4})/\eta$ [15]. Above B_c , the shape of $E_1(k_x)$ is approximately parabolic with a global minimum at $k_x = 0$. The dispersion relation $E_2(k_x)$, on the other hand, always has an approximately parabolic shape with a global minimum at $k_x = 0$.

The eigenspinors in the two subbands $E_1(k_x)$ and $E_2(k_x)$ are [15]

$$\begin{aligned}\Psi_1(B, k_x) &= \begin{bmatrix} \cos(\theta_{k_x}) \\ \sin(\theta_{k_x}) \end{bmatrix} \\ \Psi_2(B, k_x) &= \begin{bmatrix} \sin(\theta_{k_x}) \\ -\cos(\theta_{k_x}) \end{bmatrix}\end{aligned}\tag{4}$$

where $\theta_{k_x} = -(1/2)\arctan[(g^*\mu_B B)/(2\eta k_x)]$.

The fact that the eigenspinors are wavevector (k_x) dependent tells us that neither subband has a fixed spin quantization axis (the spin quantization axis changes with the wavevector). At any arbitrary k_x , each of the two spin eigenspinors in the channel will be mutually orthogonal, but each will be a mixture (or superposition) of both majority and minority spins in the ferromagnetic contacts. Moreover, at any fixed incident energy, the eigenspinors in the two spin split subbands E_1 and E_2 will not be orthogonal, so that there will be coupling between them. As a result, majority spins injected from the ferromagnet (with any arbitrary injection energy) will be mixed with minority spins in the channel. This is termed “spin mixing”. Note that spin mixing occurs because of the *simultaneous* presence of the axial magnetic field and spin orbit interaction. If the former were absent, $\theta_{k_x} = 0$, and the

eigenspinors will be z-polarized states $\begin{bmatrix} 1 \\ 0 \end{bmatrix}$ and $\begin{bmatrix} 0 \\ 1 \end{bmatrix}$ which are wavevector independent, while if the latter were absent, $\theta_{k_x} = \pi/2$ and the eigenspinors will be x-polarized states $(1/\sqrt{2}) \begin{bmatrix} 1 \\ 1 \end{bmatrix}$ and $(1/\sqrt{2}) \begin{bmatrix} 1 \\ -1 \end{bmatrix}$ which are also wavevector independent. In both of the above cases, the eigenspinors in the two subbands will be always orthogonal (at any energy) and there will be no mixing or coupling between them. Therefore, simultaneous presence of the axial magnetic field and spin orbit interaction are required to induce spin mixing.

In order to study ballistic transport in the Spin FET, we used the model developed in refs. [13, 14] to calculate the (spin-dependent) quantum mechanical transmission amplitude t of an electron through the channel (in the presence of “spin mixing”) as function of the injection energy E . For these calculations, we have used the parameters listed in Table I. The transmission amplitude $t(E)$ also depends on the axial magnetic field B and the exchange splitting Δ in the contacts. In [13, 14], we assumed that the bottoms of both majority and minority spin bands in the ferromagnet are below the Fermi level, so that both spins are propagating modes. In the present case, we modified the formalism to account for the fact that minority spins are evanescent.

From the calculated transmission amplitude as a function of energy, we calculate the linear response conductance using the finite temperature Landauer formula:

$$\begin{aligned}
G_{\uparrow}(\Delta E_c, B, \Delta) &= (e^2/4hkT) \int_{\Delta E_c}^{\infty} dE |t_{\uparrow}(E, B, \Delta)|^2 \text{sech}^2 \left(\frac{E - E_F}{2kT} \right) \\
G_{\downarrow}(\Delta E_c, B, \Delta) &= (e^2/4hkT) \int_{\Delta E_c}^{\infty} dE |t_{\downarrow}(E, B, \Delta)|^2 \text{sech}^2 \left(\frac{E - E_F}{2kT} \right) \\
G_{total}(\Delta E_c, B, \Delta) &= G_{\uparrow}(\Delta E_c, B, \Delta) + G_{\downarrow}(\Delta E_c, B, \Delta)
\end{aligned} \tag{5}$$

where \uparrow and \downarrow refer to majority and minority spins in the contact, respectively. The last equality is a consequence of the fact that in the ferromagnetic contacts, the two eigenspinors are orthogonal at any given energy. However, since the minority spin is evanescent, $G_{\downarrow}(\Delta E_c, B, \Delta) \equiv 0$, and $G_{total}(\Delta E_c, B, \Delta) = G_{\uparrow}(\Delta E_c, B, \Delta)$. We emphasize that although the evanescent modes do not directly contribute to the total conductance, they nonetheless have an *indirect* influence because they renormalize the transmission probability of the prop-

agating modes [16, 17], and therefore affect $G_{\uparrow}(\Delta E_c, B, \Delta)$ and ultimately $G_{total}(\Delta E_c, B, \Delta)$.

Because one incident mode from the contact (majority spin) is propagating, while the other (minority spin) is evanescent, the transmission spectrum $|t_{\uparrow\downarrow}|$ versus E will contain resonance/antiresonance pairs closely spaced in energy, a feature known as Fano resonances [12, 18, 19, 20]. From Equation (5), it is obvious that these Fano resonances will show up in the plot of G_{total} versus ΔE_c , at sufficiently low temperatures, for a given value of B and Δ . Note that we can vary ΔE_c with the gate voltage; therefore, a plot of G_{total} as function of gate voltage will show Fano resonances at low enough temperatures.

3 Results

In Fig. 2, we plot G_{total} versus ΔE_c at a temperature of 0 K, for different values of the exchange splitting energy Δ in the contacts. Since ΔE_c has an approximately linear dependence on the gate voltage V_g (over small ranges of gate voltage variation), this plot can also be viewed as a plot of G_{total} versus V_g . The magnetic field B along the channel is assumed to be 0.6 Tesla which is above the critical field B_c . Although η should vary with V_g , this variation is negligible over the gate voltage range we consider, since η has a weak dependence on V_g [21]. Therefore, we assume that η is constant over the entire range of ΔE_c (or V_g) and has the value given in Table I.

In Fig. 2, we clearly see the Fano resonance-antiresonance pairs. Additionally, there are isolated resonances where the conductance reaches the maximum value of e^2/h . These are due to Ramsauer resonances discussed in ref. [13]. The locations of the Ramsauer resonances (on the ΔE_c axis) are fairly insensitive to the exchange splitting energy Δ , but the locations of the Fano resonance-antiresonance pairs are strongly dependent on Δ . This is due to the fact that the decay length of the evanescent minority spin band in the contact has a strong dependence on Δ . The value of Δ affects the amount of coupling/mixing between the two propagating modes in the semiconductor channel via the boundary conditions at the contacts. That, in turn, affect the Fano resonances, but not the Ramsauer resonances.

The energy separation between the Fermi level and the subband bottoms depends on the axial magnetic field B . Therefore, we expect the magnetic field to influence the Fano resonances, and it does. This is illustrated in Fig. 3 which is a plot of G_{total} versus ΔE_c for different values of the axial magnetic field B for a fixed value of $\Delta = 6$ eV. For the range of ΔE_c considered here, there are two Ramsauer resonances. In addition, there is a Fano resonance preceding each Ramsauer resonance. The Ramsauer resonances correspond to perfect transmission of the majority spin band, while each Fano resonance appears in place of a second Ramsauer resonance that would have appeared owing to perfect transmission of the minority spin band, were it propagating instead of being evanescent.

Around a Fano resonance, a very small change in ΔE_c will switch the conductance from the maximum value of e^2/h to zero. Therefore, we can realize a *binary switch* by biasing the device close to a Fano resonance. This can be achieved by applying an appropriate fixed dc voltage on the gate. Around the leftmost Fano resonance, the change in ΔE_c ($\delta(\Delta E_c)$) required to switch the device on or off, is $\sim 20 \mu\text{eV}$ and is nearly independent of the strength of the magnetic field B . Since $\delta(\Delta E_c) = qV_g - qV_{ins}$ (where V_g is the gate voltage, q is the electronic charge and V_{ins} is the gate voltage dropped across the gate insulator), the gate voltage swing V_t required to switch the device from on-to-off is $20 \mu\text{V} + V_{ins}$. For acceptable error rate, we want this voltage to exceed the thermal noise voltage on the gate capacitor, which is $U_{th} = \sqrt{kT/C_g}$, where C_g is the gate capacitance and T is the operating temperature [22]. We will later show that the Fano resonances begin to wash out at temperatures above 0.1 K, so that $T \leq 0.1$ K. Assuming $C_g = 1$ fF (including interconnects), $U_{th} \leq 37 \mu\text{V}$. Therefore, we must choose the gate insulator such that $V_{ins} \geq 17 \mu\text{V}$.

If the gate capacitance is 1 fF (including interconnects), then the energy dissipated in switching this transistor is $(1/2)CV_t^2 = 7 \times 10^{-25}$ Joules $\approx kT \ln 2$ (at the temperature of 0.1 K). If switched adiabatically, the energy dissipation can be much less [23]. Consequently, the binary switch that we propose here is an extremely *low power* switch.

Near a Ramsauer resonance (perfect transmission of the majority spin band), the con-

ductance versus ΔE_c curve is fairly insensitive to the axial magnetic field B . However, near a Fano resonance, the conductance curve is extremely sensitive to B . For instance, at zero temperature, when the gate is biased close to a Fano resonance (at a voltage such that $\Delta E_c = 4.1922$ eV), there is a 100% change in the conductance (from a maximum value of e^2/h to zero) when the magnetic field B is changed from 0.4 T to 0.372 T, a mere change of 28 mT. Therefore, at very low temperatures, this device can operate as a magnetic field sensor. We show below that it can actually detect fields with a sensitivity of ~ 1 femto-Tesla/ \sqrt{Hz} , using standard analysis as in refs. [24, 25].

4 Magnetic field sensor

Consider a single device. The noise current has two components - thermal noise and shot noise. The thermal noise current is given by $I_n^{thermal} = \sqrt{4kTG\Delta f}\zeta$, where G is the source-to-drain conductance, Δf is the frequency bandwidth, and ζ is the noise suppression factor due to carrier confinement in quantum wires [26]. The shot noise current is $I_n^{shot} = \sqrt{(2/3)eGV\Delta f}$ [27]. Therefore the total noise current in a transistor is $I_n = C\sqrt{G}$, where $C = \sqrt{[4kT\zeta^2 + (2/3)eV]\Delta f}$.

When used as a magnetic field sensor, the change in the current through a single transistor in a magnetic field H is the signal current I_s and is given by $I_s = SH$ where S is the sensitivity. To keep the analysis tractable, we will assume that current changes linearly in a magnetic field, so that S is independent of H . Therefore, the signal to noise ratio (SNR) for a single transistor is

$$SNR = \frac{SH}{I_n^{thermal} + I_n^{shot}} = \frac{SH}{C\sqrt{G}} \quad (6)$$

The conductance of N transistors operating in parallel is NG . Therefore, the noise current of N transistors in parallel is $\sqrt{N}I_n$, whereas the signal current is NI_s . Thus, the SNR increases as \sqrt{N} . This allows us to detect very small magnetic fields by using a large number of transistors in parallel, each acting as a sensor.

For a change of magnetic field of 28 mTesla \equiv 280 Oe, the conductance of a transistor

changes by e^2/h . If the source-to-drain voltage is 100 mV, then the drain current changes by $39 \mu\text{A}$. Therefore $S = 0.14 \mu\text{A/Oe}$. For a field of 1 femto-Tesla $= 10^{-11}$ Oe, the signal current I_s in a single transistor is 1.4×10^{-18} Amperes. The noise current is dominated by shot noise at the operating temperature of 0.1 K and is given by 6.4×10^{-13} Amperes/ $\sqrt{\text{Hz}}$. Therefore, the SNR for a single transistor is $2.2 \times 10^{-6}/\sqrt{\text{Hz}}$. The SNR for 2.5×10^{11} transistor sensors in parallel will be $\sqrt{2.5 \times 10^{11}}$ times larger and exceed unity/ $\sqrt{\text{Hz}}$ (0 db), which makes the signal measurable against the background of noise. Therefore with an array of $500,000 \times 500,000$ transistors, we should be able to detect a magnetic field of 1 femto-Tesla with a bandwidth of 1 Hz. With a transistor density of $2.5 \times 10^9/\text{cm}^2$, this sensor can be implemented in a $10 \text{ cm} \times 10 \text{ cm}$ chip. The dynamic power dissipated to detect 1 femto-Tesla (in a bandwidth of 1 Hz) will be only 35 nWatts.

In Fig. 4, we show that the Fano resonances wash out very quickly with increasing temperature. The Ramsauer resonances are more robust against temperature. The Fano resonances are essentially indiscernible at temperatures above 0.3 K, so that we should restrict all device operation to below 0.1 K.

5 Conclusion

In conclusion, we have shown that a Spin FET with *half metallic* contacts has both Ramsauer and Fano resonances in the transmission spectrum. In ref. [13], we found only the Ramsauer resonances, and not the Fano resonances, since we did not consider half metallic ferromagnetic contacts, so that both majority and minority spins in the contact were propagating modes. Here, we have considered the case where the majority spins are propagating, but the minority spins are evanescent. This causes the Fano resonances. The locations of the Fano resonances are very sensitive to an axial magnetic field and the exchange splitting in the contacts. We can bias the transistor near a Fano resonance using a dc gate voltage and, at low temperatures, realize very low power binary switches (dissipating $\sim kT \ln 2$ energy per switching event), as well as sensitive magnetic field detectors that can detect ultrasmall

fields with a sensitivity ~ 1 femto-Tesla/ \sqrt{Hz} .

References

- [1] S. Datta and B. Das, Appl. Phys. Lett., **56**, 665 (1990).
- [2] J. Schliemann, J. C. Egues and D. Loss, Phys. Rev. Lett., **90**, 146801 (2003).
- [3] X. Cartoixá, D. Z-Y Ting and Y-C Chang, Appl. Phys. Lett., **83**, 1462 (2003).
- [4] K. C. Hall and M. E. Flatté, Appl. Phys. Lett., **88**, 162503 (2006).
- [5] A. R. Trivedi, S. Bandyopadhyay and M. Cahay (unpublished).
- [6] R. Fiederling, M. Keim, G. Reuscher, W. Ossau, G. Schmidt, A. Waag and L. W. Molenkamp, Nature (London), **402**, 787 (1999).
- [7] R. A. de Groot, F. M. Mueller, P. G. van Engen and K. H. J. Buschow, Phys. Rev. Lett., **50**, 2024 (1983).
- [8] W. E. Pickett and J. S. Moodera, Phys. Today, **54**, 39 (2001).
- [9] S. Sanvito and N. A. Hill, Phys. Rev. Lett., **87**, 267202 (2001).
- [10] R. J. Elliott, Phys. Rev., **96**, 266 (1954).
- [11] M. I. D'yakonov and V. I. Perel', *Sov. Phys. Solid State*, **13**, 3023 (1972).
- [12] U. Fano, Phys. Rev. **124**, 1866 (1961).
- [13] M. Cahay and S. Bandyopadhyay, Phys. Rev. B, **68**, 115316 (2003).
- [14] M. Cahay and S. Bandyopadhyay, Phys. Rev. B, **69**, 045303 (2004).
- [15] S. Bandyopadhyay, S. Pramanik and M. Cahay, Superlat. Microstruct., **35**, 67 (2004).
- [16] P. F. Bagwell, Phys. Rev. B, **41**, 10354 (1990).
- [17] M. Cahay, S. Bandyopadhyay, M. A. Osman and H. L. Grubin, Surface Science, **228**, 301 (1990).

- [18] P.F. Bagwell and R.K. Lake, Phys. Rev. B, **46**, 15329 (1992).
- [19] C. Kunze and P.F. Bagwell, Physical Review B, **51**, 13410, (1995).
- [20] L. Serra and D. Sánchez, www.arXiv.org/cond-mat/0610147.
- [21] J. Nitta, T. Akazaki, H. Takayanagi and T. Enoki, Phys. Rev. Lett., **78**, 1335 (1997).
- [22] Laszlo B. Kish, Phys. Lett. A, **305**, 144 (2002).
- [23] R. K. Cavin, V. V. Zhirnov, J. A. Hutchby and G. I. Bourianoff, Fluctuations and Noise Letters, **5**, C29 (2005).
- [24] M. Tondra, J. M. Daughton, D. Wang, R. S. Beech, A. Fink and J. A. Taylor, J. Appl. Phys., **83**, 6688 (1998).
- [25] S. Bandyopadhyay and M. Cahay, Physica E, **27**, 98 (2005).
- [26] A. Svizhenko, S. Bandyopadhyay and M. A. Strosio, J. Phys.: Condens. Matt., **11**, 3697 (1999).
- [27] C. W. J. Beenakker and M. Büttiker, Phys. Rev. B, **46**, 1889 (1992).

Table I: Parameters of the spin interferometer

Fermi Energy E_F (eV)	4.2
Rashba spin-orbit coupling constant α_R (10^{-11} eVcm)	1.
Lande Factor g^*	-14.9
Effective mass m_f^* in Fe contact (m_0)	1.
Effective mass m_s^* in InAs channel (m_0)	0.023
Length of the channel(μm)	0.15
Strength of delta scatterer at the contact/channel interface (ev \AA)	2.0

Figure 1: (a) Structure of a Spin Field Effect Transistor with half metallic (HM) source and drain contacts. (b) Energy band diagram along the channel: Also shown as dashed lines are the resonant energy states above ΔE_c . The barriers at the ferromagnet/semiconductor interface are modeled as simple one-dimensional delta-potentials.

Figure 2: Zero temperature conductance G_{total} ($=G_{\uparrow}$) as a function of ΔE_c for various values of the exchange energy Δ in the half-metallic contacts. The axial magnetic field $B = 0.6$ Tesla. Other parameters used to obtain these curves are listed in Table I.

Figure 3: Zero temperature conductance G_{total} ($=G_{\uparrow}$) as a function of ΔE_c for various values of the axial magnetic field B . The exchange energy Δ in the half-metallic contacts is assumed to be 6 eV. The Fano and Ramsauer resonances are indicated.

Figure 4: (a) Temperature dependence of the conductance modulation of the Spin FET when the exchange energy Δ in the half-metallic contacts is 6 eV. The Fano resonances are washed out much faster than the Ramsauer resonances as the temperature rises. (b) Temperature dependence of the leftmost Fano resonance shown in higher resolution. From top to bottom, the curves correspond to a temperature of 0, 0.05, 0.1, 0.15, 0.2, 0.25, and 0.3 K, respectively.

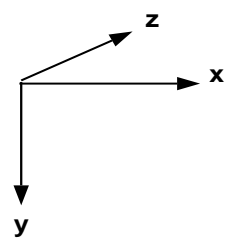
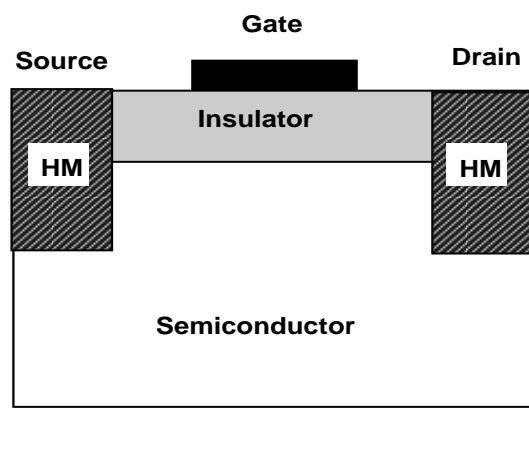


Figure 1(a)

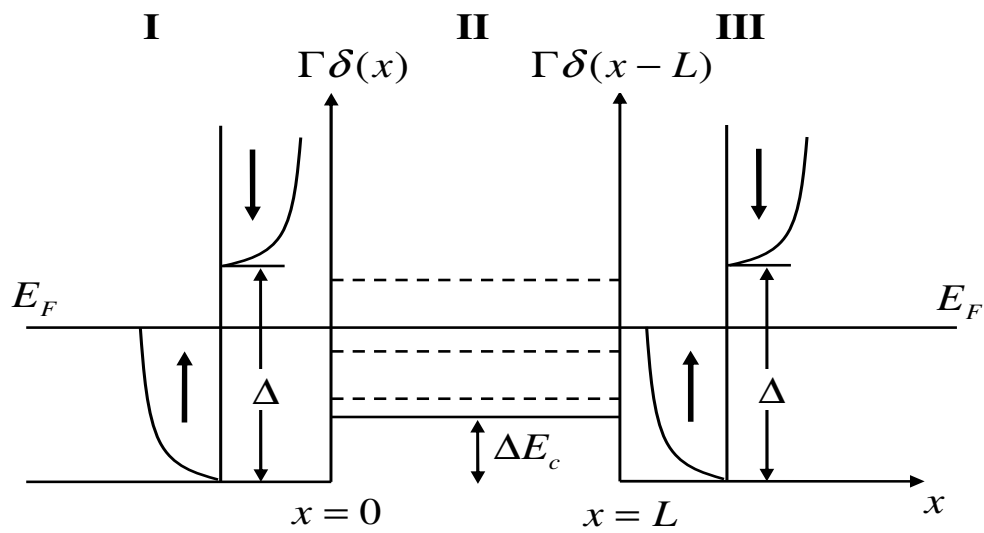


Figure 1(b)

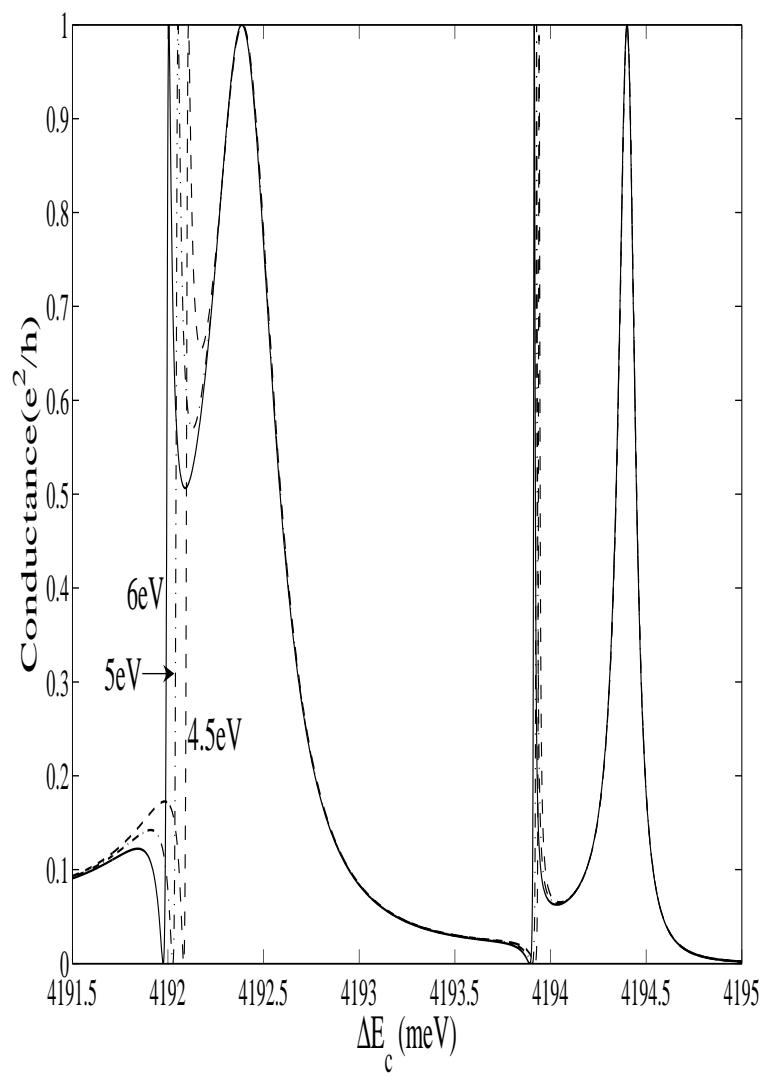


Figure 2

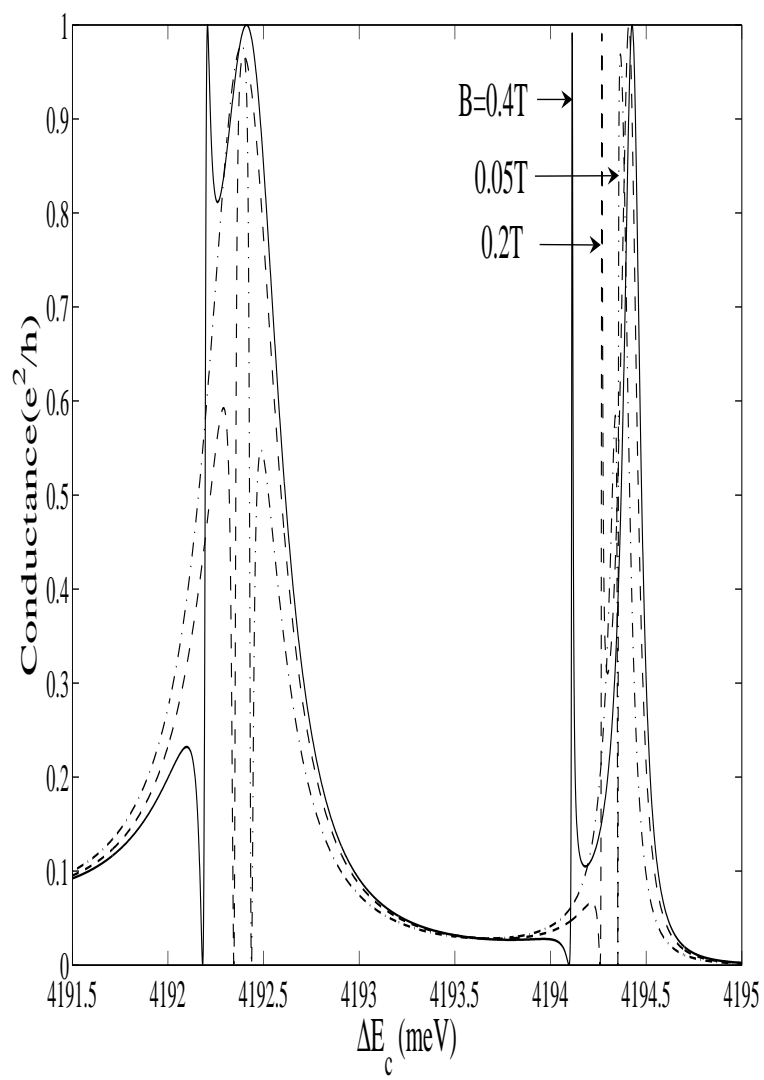


Figure 3

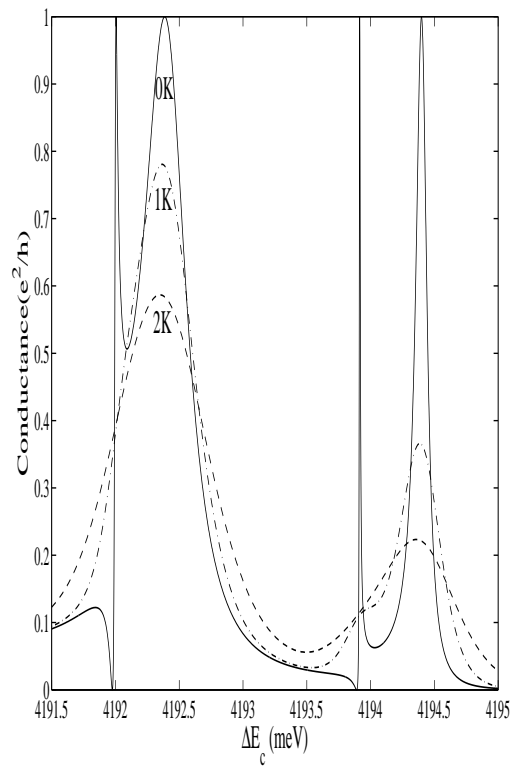


Figure 4(a)

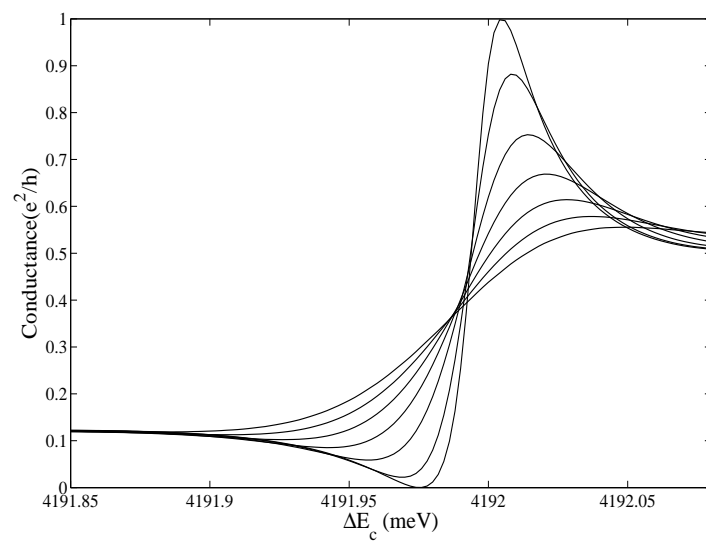


Figure 4(b)